Inorganic Chemistry

ARTICLE

pubs.acs.org/IC

Manganese(III)-Containing Wells–Dawson Sandwich-Type Polyoxometalates: Comparison with their Manganese(II) Counterparts

Mounim Lebrini,[†] Israël M. Mbomekallé,*[,†] Anne Dolbecq,[†] Jérôme Marrot,[†] Patrick Berthet,[‡] Joseline Ntienoue,[†] Francis Sécheresse,[†] Jacky Vigneron,[†] and Arnaud Etcheberry[†]

[†]Institut Lavoisier de Versailles, UMR 8180, CNRS Université de Versailles Saint-Quentin, 45 Avenue des Etats-Unis, 78035 Versailles Cedex, France

[‡]Laboratoire de Physico-Chimie de l'Etat Solide, ICMMO, UMR 8182, CNRS, Université Paris-Sud, Bâtiment 410, 91405 Orsay Cedex, France

Supporting Information

ABSTRACT: We present the synthesis and structural characterization, assessed by various techniques (FTIR, TGA, UV–vis, elemental analysis, single-crystal X-ray diffraction for three compounds, magnetic susceptibility, and electrochemistry) of five manganese-containing Wells–Dawson sandwich-type (WDST) complexes. The dimanganese(II)-containing complex, $[Na_2(H_2O)_2Mn^{II}{}_2(As_2W_{15}O_{56})_2]^{18-}$ (**1**), was obtained by reaction of $MnCl_2$ with 1 equiv of $[As_2W_{15}O_{56}]^{12-}$ in acetate medium (pH 4.7). Oxidation of **1** by $Na_2S_2O_8$ in aqueous solution led to the dimanganese(III) complex $[Na_2(H_2O)_2Mn^{III}{}_2(As_2W_{15}O_{56})_2]^{16-}$ (**2**), while its trimanganese(II) homologue, $[Na(H_2O)_2Mn^{II}(H_2O)Mn^{II}{}_2(As_2W_{15}O_{56})_2]^{17-}$ (**3**), was obtained by addition of ca. 1 equiv of $MnCl_2$ to a solution of **1** in 1 M NaCl. The trimanganese(III) and tetramanganese(III) counterparts, $[Mn^{III}(H_2O)Mn^{III}{}_2(As_2W_{15}O_{56})_2]^{15-}$ (**4**) and $[Mn^{III}{}_2(H_2O)_2Mn^{III}{}_2(As_2W_{15}O_{56})_2]^{12-}$ (**6**), are, respectively, obtained by oxidation of aqueous solutions of **3** and $[Mn^{II}{}_2(H_2O)_2Mn^{II}{}_2(As_2W_{15}O_{56})_2]^{16-}$ (**5**) by $Na_2S_2O_8$. Single-crystal X-ray analyses were carried out on **2**, **3**, and **4**. BVS calculations and XPS confirmed that the oxidation state of Mn centers is +II for complexes **1**, **3**, and **5** and +III for **2**, **4**, and **6**. A complete comparative electrochemical study was carried out on the six compounds cited above, and it was possible to observe the distinct redox steps $Mn^{IV/III}$ and $Mn^{III/II}$. Magnetization measurements, as a function of temperature, confirm the presence of antiferromagnetic interactions between the Mn ions in these compounds in all cases with the exception of compound **2**.

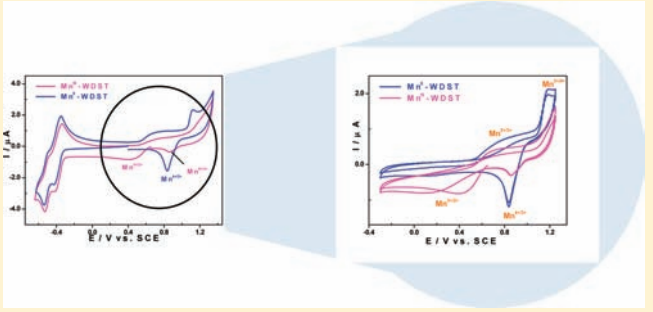

INTRODUCTION

The chemistry of polyoxometalates (POMs) continues to attract much attention. In fact, these molecules display a multitude of properties based on their highly alterable sizes, shapes, charge densities, and reversible redox potentials.[1,2] As a consequence, possible applications span a wide range of domains including catalysis, electrocatalysis, medicine, materials science, photochemistry, analytical chemistry, and magnetochemistry.[3−7] Frequently novel polyoxoanions with unexpected structures are discovered, which can be traced to the fact that the mechanism of formation of polyoxometalates is not well understood and is commonly described as self-assembly. Therefore, it is necessary to systematically analyze the complex equilibria of polyoxometalates in order to eventually design straightforward syntheses of novel species. The dual objective is to develop efficient, rational, and new synthetic routes for POMs that are likely to play a major role in both catalysis and magnetism, as well as to understand and therefore control the mechanism of their formation. In this context, the Wells–Dawson sandwich-type (WDST) complexes are of both practical and intellectual interest.[8] They are derived from the reaction of the lacunary Wells–Dawson species, $[X_2W_{15}O_{56}]^{12-}$ (where X = As or P), and a d-metal cation, M (where M = Mn^{II}, Fe^{II}, Fe^{III}, Co^{III}, Ni^{II}, Cu^{II}, Zn^{II} or Cd^{II}), which usually leads to the complex anion $[M_4(H_2O)_2(X_2W_{15}O_{56})_2]^{y-}$, in which the $M_4O_{14}(H_2O)_2$ metal cluster is sandwiched by the two lacunary fragments. The presence of the $M_4O_{14}(H_2O)_2$ metal cluster makes these complexes useful for applications in both catalysis and magnetism.[9] One can easily imagine a selective incorporation of the diverse metals M to obtain the desired magnetic or catalytic properties.

Here, we report, for the first time, the synthesis and structural characterization, by single-crystal X-ray analysis whenever possible, of five novel manganese-containing sandwich-type

Received: November 8, 2010
Published: June 20, 2011

complexes. The dimanganese(II)-containing sandwich-type complex $[Na_2(H_2O)_2Mn^{II}{}_2(As_2W_{15}O_{56})_2]^{18-}$ (**1**) was obtained through a synthesis we only newly developed.[10] Oxidation of **1** by $Na_2S_2O_8$ in aqueous solution led to the dimanganese(III) sandwich-type complex $[Na_2(H_2O)_2Mn^{III}{}_2(As_2W_{15}O_{56})_2]^{16-}$ (**2**), while its trimanganese(II) homologue, $[Na(H_2O)_2Mn^{II}(H_2O)Mn^{II}{}_2(As_2W_{15}O_{56})_2]^{17-}$ (**3**), was obtained by addition of ca. 1 equiv of $MnCl_2$ to a solution of **1** in 1 M NaCl. The trimanganese(III), $[Mn^{III}(H_2O)Mn^{III}{}_2(As_2W_{15}O_{56})_2]^{15-}$ (**4**), and tetramanganese(III), $[Mn^{III}{}_2(H_2O)_2Mn^{III}{}_2(As_2W_{15}O_{56})_2]^{12-}$ (**6**), counterparts were obtained by oxidation of aqueous solutions of **3** and $[Mn^{II}{}_2(H_2O)_2Mn^{II}{}_2(As_2W_{15}O_{56})_2]^{16-}$ (**5**),[8m] respectively, with $Na_2S_2O_8$. Examples of manganese(III)-containing Keggin sandwich-type complexes are described and used in several catalytic or electrocatalytic processes,[11] but to the best of our knowledge, this is the first case of manganese(III) WDST to be described and fully characterized. All six complexes were characterized by elemental analysis, thermal gravimetric analysis (TGA), infrared spectroscopy (IR), UV−vis spectroscopy, X-ray photoelectron spectroscopy (XPS), magnetic susceptibility, and electrochemistry.

EXPERIMENTAL SECTION

General Methods and Materials. Pure water was used throughout. It was obtained by passing water through a RiOs 8 unit followed by a Millipore-Q Academic purification set. All reagents were of high-purity grade and used as purchased without further purification. Elemental analysis was performed by the Service Central d'Analyse CNRS Solaize, France. Water content corresponding to weight loss up to about 250 °C was determined by thermal gravimetric analysis (TGA) by using a TGA-7 Perkin-Elmer apparatus. IR spectra were recorded with KBr pellets on a Nicolet Magna IR Spectrometer 550 spectrophotometer. UV−vis spectra were recorded on a Perkin-Elmer Lambda 19 spectrophotometer on 2.5×10^{-5} M solutions of the relevant polyanion. Matched 1.000 mm optical path quartz cuvettes were used. The compositions of the various media were as follows: 0.2 M Na_2SO_4 + H_2SO_4, pH 1, 2, and 3, and 0.4 M CH_3COONa + CH_3COOH, pH 4, 5, and 6. XPS surface chemical analyses were achieved with a Thermo Electron K-Alpha spectrometer using a monochromatic Al Kα X-ray source (1486.6 eV). Charge compensation was used to overcome the charging effects. Acquisition parameters imposed in this study are as follows: 400 × 400 μm spot size, 12 kV primary energy, 6.0 mA emission intensity, CAE mode (50 eV), and 0.15 eV energy step size. Magnetic measurements were carried out on polycrystalline samples using a SQUID magnetometer, Quantum Design MPMS-5.

Syntheses. The starting sample of $Na_{12}[As_2W_{15}O_{56}]\cdot 21H_2O$ was obtained by published procedures, and purity was confirmed by IR and cyclic voltammetry.[12]

*Synthesis of $Na_{18}[Na_2(H_2O)_2Mn^{II}{}_2(As_2W_{15}O_{56})_2]\cdot 33H_2O$ (**1**).* A 10.00 g (2.24 mmol) sample of $Na_{12}[As_2W_{15}O_{56}]\cdot 21\ H_2O$ was suspended in 50 mL of a 0.5 M CH_3COONa/0.5 M CH_3COOH buffer (pH 4.6). Then 0.43 g (2.17 mmol) of $MnCl_2\cdot 4H_2O$ was added in small portions at room temperature. After about 15 min any insoluble material was filtered off and the clear filtrate was treated with 10 g (0.17 mol) of solid NaCl. The pale brown crystalline precipitate formed was collected by filtration, washed twice with 1 M NaCl and with ethanol, dried in the open air (4.12 g; 77.8%), and found to correspond to $Na_{18}[Na_2(H_2O)_2Mn^{II}{}_2(As_2W_{15}O_{56})_2]\cdot 33H_2O$. IR (1% KBr pellet, 1000−300 cm^{-1}): 996(vw); 940(s); 870(m); 802 (m); 789(vw); 758(w); 712(m); 519(m); 493(m); 474(vw); 431(w); 386(vw); 353(m); 322(w). Anal. Calcd (found) for $Na_{18}[Na_2(H_2O)_2Mn^{II}{}_2(As_2W_{15}O_{56})_2]\cdot 33H_2O$: As, 3.40 (3.24); W, 62.63 (60.27); Mn, 1.25 (1.23); Na, 5.22 (5.78). MW 8807.06.

*Synthesis of $Na_{16}[Na_2(OH_2)_2Mn^{III}{}_2(As_2W_{15}O_{56})_2]\cdot 50H_2O$ (**2**).* A 1.60 g (0.18 mmol) sample of **1** (synthesized as described above) was dissolved in 50 mL of a 0.5 M CH_3COONa/0.5 M CH_3COOH buffer, pH 4.6. Then 0.5 g (0.21 mmol) of $Na_2S_2O_8$ was added, and the solution was heated at 80 °C for 2 h. The solution color changed from orange to dark brown. The solution was then filtered while hot, treated with 2 g (0.034 mol) of solid NaCl, and left open to the air at room temperature. After 1 day, the dark brown crystals formed were collected by filtration, washed twice with 1 M NaCl and then with ethanol, dried in the open air (0.75 g; 45.4%), and found to correspond to the compound $Na_{16}[Na_2(OH_2)_2Mn^{III}{}_2(As_2W_{15}O_{56})_2]\cdot 50H_2O$. IR (1% KBr pellet, 1000−300 cm^{-1}): 999(vw); 945(s); 873(m); 818(m); 760(w); 723(m); 520(m); 493(w); 474(vw); 428(w); 383(vw); 354(m); 318(w). Anal. Calcd (found) for $Na_{16}[Na_2(OH_2)_2Mn^{III}{}_2(As_2W_{15}O_{56})_2]\cdot 50H_2O$: As, 3.31 (3.32); W, 60.83 (59.66); Mn, 1.21 (1.27); Na, 4.57 (4.65). MW 9067.06.

*Synthesis of $Na_{17}[Na(H_2O)Mn^{II}(H_2O)Mn^{II}{}_2(As_2W_{15}O_{56})_2]\cdot 55H_2O$ (**3**).* To a solution containing 15 mg (0.08 mmol) of $MnCl_2\cdot 4H_2O$ in 20 mL of 0.5 M aqueous NaCl was added in small portions, under stirring and heating (65 °C), 0.50 g (0.06 mmol) of **1** (synthesized as described above). The solution was heated for about 30 min and then filtered while hot. The orange and clear filtrate was left at room temperature. The brown crystalline material that formed was collected by filtration, washed twice with 1 M NaCl and then with ethanol, dried in the open air (0.36 g; 73%), and found to correspond to the compound $Na_{17}[Na(H_2O)Mn^{II}(H_2O)Mn^{II}{}_2(As_2W_{15}O_{56})_2]\cdot 55H_2O$. IR (1% KBr pellet, 1000−300 cm^{-1}): 998(vw); 941(s); 873(m); 813(m); 789(vw); 764(w); 715(m); 520(m); 491(m); 472(vw); 431(w); 386(vw); 356(m); 328(w). Anal. Calcd (found) for $Na_{17}[Na(H_2O)Mn^{II}(H_2O)Mn^{II}{}_2(As_2W_{15}O_{56})_2]\cdot 55H_2O$: As, 3.49 (3.31); W, 64.2 (62.34); Mn, 1.92 (1.97); Na, 4.28 (5.08). MW 9212.

*Synthesis of $Na_{15}[Mn^{III}(H_2O)Mn^{III}{}_2(As_2W_{15}O_{56})_2]\cdot 55H_2O$ (**4**).* To a solution containing 18 mg (0.09 mmol) of $MnCl_2\cdot 4H_2O$ in 20 mL of 0.5 M aqueous NaCl was added in small portions, under stirring and heating (65 °C), 0.50 g (0.06 mmol) of **1** (synthesized as described above). The solution was heated for about 30 min; then 30 mg (0.13 mmol) of $Na_2S_2O_8$ was added. The temperature was held at 80 °C for about 2 h. During this time, the color of the solution changed from orange to dark brown. The solution was filtered while still hot and left in the open air at room temperature. The brown crystalline material formed was collected by filtration, washed twice with 1 M NaCl and then ethanol, and dried in the open air (0.26 g; 52.6%) corresponding to the compound $Na_{15}[Mn^{III}(H_2O)Mn^{III}{}_2(As_2W_{15}O_{56})_2]\cdot 55H_2O$. IR (1% KBr pellet, 1000−300 cm^{-1}): 1000(vw); 953(s); 875(m); 830(m); 779(w); 732(m); 520(m); 490(w); 472(vw); 425(w); 388(vw); 358(m); 316(w). Anal. Calcd (found) for $Na_{15}[Mn^{III}(H_2O)Mn^{III}{}_2(As_2W_{15}O_{56})_2]\cdot 55H_2O$: As, 3.34 (3.26); W, 61.5 (60.2); Mn, 1.84 (1.88); Na, 3.85(4.20). MW 9125.

*Synthesis of $Na_{12}[Mn^{III}{}_2(H_2O)_2Mn^{III}{}_2(As_2W_{15}O_{56})_2]\cdot 60H_2O$ (**6**).* A 2.0 g (0.22 mmol) sample of $Na_{14}[Mn^{II}{}_2(H_2O)_2Mn^{II}{}_2(As_2W_{15}O_{56})_2]\cdot 55H_2O$ (**5**) (synthesized as described in ref 8m) was dissolved in 50 mL of a 1 M NaCl. Then 1.25 g (5.2 mmol) of a $Na_2S_2O_8$ was added, and the solution was heated at 80 °C for two 4 h. The solution color changed from pale to dark brown. The solution was filtered while still hot, and the fine dark powder formed was eliminated. The dark brown clear solution was left to evaporate in the air at room temperature. After 1 day, the dark brown crystals that formed were collected by filtration, washed twice with 1 M NaCl and ethanol, and dried in the open air (1.36 g; 67.3%). They were found to correspond to the compound $Na_{12}[Mn^{III}{}_2(H_2O)_2Mn^{III}{}_2(As_2W_{15}O_{56})_2]\cdot 60H_2O$. IR (1% KBr pellet, 1000−300 cm^{-1}): 1000(vw); 947(s); 873(m); 822(m); 766(w); 723(m); 524(m); 492(w); 472(vw); 425(w); 383(vw); 352(m); 316(w). Anal. Calcd (found) for $Na_{12}[Mn^{III}{}_2(H_2O)_2Mn^{III}{}_2(As_2W_{15}O_{56})_2]\cdot 60H_2O$: As, 3.25 (3.20); W, 59.8 (59.3); Mn, 4.12

dx.doi.org/10.1021/ic102237x |Inorg. Chem. 2011, 50, 6437–6448

Table 1. Crystallographic Data for 2, 3, and 4

	2	3	4
empirical formula	$H_{104}As_4Mn_2Na_{18}O_{164}W_{30}$	$H_{114}As_4Mn_3Na_{16}O_{169}W_{30}$	$H_{112}As_4Mn_3Na_{15}O_{168}W_{30}$
fw, g	9067.71	9166.75	9125.75
cryst syst	monoclinic	monoclinic	triclinic
space group	$P2_1/c$	$P2_1/c$	P-1
a/Å	17.0151(7)	17.143(3)	12.733(5)
b/Å	15.2570(7)	15.096(3)	15.855(7)
c/Å	31.9120(15)	31.480(6)	19.475(8)
α/deg	90	90	87.59(2)
β/deg	91.294(3)	90.41(1)	83.89(2)
γ/deg	90	90	75.20(2)
V/Å^3	8282.2(6)	8147(3)	3779(3)
Z	2	2	1
ρ_{calc}/g cm^{-3}	3.636	3.737	4.010
μ/mm^{-1}	21.840	22.276	24.005
data/parameters	24433/780	23982/1027	21844/971
R_{int}	0.0774	0.0672	0.0298
GOF	1.032	1.107	1.003
R ($>2\sigma(I)$)	R_1 = 0.0956	$R_1{}^a$ = 0.0675	R_1 = 0.0802
	wR_2 = 0.2487	$wR_2{}^b$ = 0.1868	wR_2 = 0.2350

$^a R_1 = (\Sigma||F_o| - |F_c||)/(\Sigma|F_c|)$. $^b wR_2 = ((\Sigma w(F_o^2 - F_c^2)^2)/(\Sigma w(F_o^2)^2))^{1/2}$.

(3.98); Na, 2.99 (3.24). Found: As, 3.20; W, 59.3; Mn, 3.98; Na, 3.24. MW 9218.94.

X-ray Crystallography. Intensity data collection was carried out with a Bruker Nonius X8 APEX 2 diffractometer equipped with a CCD bidimensional detector using the monochromatized wavelength λ(Mo Kα) = 0.71073 Å. The data were collected at room temperature for **2** and **4** and at 100 K for **3**, whose crystals are unstable due to loss of water of hydration. The absorption correction was based on multiple and symmetry-equivalent reflections in the data set using the SADABS program[13] based on the method of Blessing.[14] The structures were solved by direct methods and refined by full-matrix least squares using the SHELX-TL package.[15] As usually observed for structures of polyoxometalates, which are large and highly negatively charged entities, it has not been possible to locate all the water molecules and alkali counterions because of disorder.[16] As a consequence, in all the structures there is a discrepancy between the formulas determined by elemental analysis and the formulas deduced from the crystallographic atom list. In particular, in the structure of **2**, the position of 2 sodium ions and 12 hydration water molecules could not be determined from the Fourier difference map, even if the structure was registered at low temperature (3 °C). Elemental analysis for Na for this compound provides additional evidence for the sodium composition. This produces an alert A in the checkcif report about very large solvent accessible void, not unusal in the structures of POMs. Crystallographic data are given in Table 1. Comparisons of selected bond lengths are given in Table 2.

Electrochemical Experiments. The same media as for UV−vis spectroscopy were used for electrochemistry, but the polyanion concentration was 2×10^{-4} M. All cyclic voltammograms were recorded at a scan rate of 10 mV s^{-1} unless otherwise stated. The solutions were deaerated thoroughly for at least 30 min with pure argon and kept under a positive pressure of this gas during the experiments. The source, mounting, and polishing of the glassy carbon (GC, Le Carbone Lorraine, France) electrodes has been described.[17] The glassy carbon samples had a diameter of 3 mm. The electrochemical setup was an EG&G 273 A driven by a PC with the M270 software. Potentials are quoted against a saturated calomel electrode (SCE). The counter electrode was platinum gauze of large surface area. All experiments were performed at room temperature.

Table 2. Selected Bond Lengths (Å) and Valence Bond Summations (Σ_s) for 2, 3, 4, and 5[8m] Associated to the Representations in Figure 2

2					
Mn1−O41	1.93(3)	Na1−O48	2.21(2)	A···A′	5.988(18)
Mn1−O36	1.95(2)	Na1−O52	2.31(2)	B···B′	3.194(5)
Mn1−O45	1.98(2)	Na1−O56	2.38(2)		
Mn1−O55	2.08(2)	Na1−O41	2.39(3)		
Mn1−O56	2.10(2)	Na1−O2W	2.43(7)		
Mn1−O56	2.23(2)	Na1−O36	2.51(2)		
Σ_s(Mn1)	2.88				
3					
Mn1−O45	2.086(10)	Mn2−O48	2.173(11)	Na2−O57	2.20(2)
Mn1−O55	2.111(8)	Mn2−O52	2.192(10)	Na2−O41	3.06(3)
Mn1−O36	2.136(9)	Mn2−O41	2.286(11)	Na2−O36	2.25(2)
Mn1−O41	2.155(9)	Mn2−O56	2.293(10)	Na2−O52	2.33(2)
Mn1−O56	2.215(9)	Mn2−O36	2.313(10)	Na2−O48	2.35(3)
Mn1−O56	2.218(9)	Mn2−O57	2.353(14)	Na2−O56	2.37(2)
Σ_s(Mn1)	2.26	Σ_s(Mn2)	1.67	A···A′	5.77(3)
				B···B′	3.401(3)
4					
Mn1−O54	1.920(6)	Mn2−O51	1.901(6)	A···A′	5.40(4)
Mn1−O39	1.922(5)	Mn2−O41	1.911(7)	B···B′	3.06(3)
Mn1−O45	1.929(5)	Mn2−O56	2.040(7)		
Mn1−O49	1.933(6)	Mn2−O56	2.075(7)		
Mn1−O57	2.198(6)	Mn2−O45	2.282(6)		
Mn1−O56	2.239(6)	Mn2−O49	2.243(8)		
Σ_s(Mn1)	3.13	Σ_s(Mn2)	2.76		
5					
Mn1−O48	2.092(9)	Mn2−O49	2.074(9)	A···A′	5.674(4)
Mn1−O47	2.126(9)	Mn2−O52	2.099(9)	B···B′	3.396(4)
Mn1−O50	2.157(9)	Mn2−O50	2.156(8)		
Mn1−O1W	2.195(10)	Mn2−O51	2.157(9)		
Mn1−O51	2.198(8)	Mn2−O53	2.230(9)		
Mn1−O53	2.241(8)	Mn2−O53	2.243(8)		
Σ_s(Mn1)	2.17	Σ_s(Mn2)	2.24		

RESULTS AND DISCUSSION

Syntheses. A few years ago, we launched a series of experimental studies that explored and attempted to explain mechanisms that govern the formation of POMs and their substituted "d" and "f" derivatives.[18] The purpose of this research program was to develop simple and rational procedures that improve synthesis of new or well-known POMs.[19] In a previous paper,[10] we presented and widely discussed the conditions of obtaining isomerically pure samples of lacunary WDST complexes, i.e., those containing less than four "d" metal centers, which were likely to incorporate supplementary metallic centers. The present study will therefore focus on comparing the physical properties of six manganese-containing WDST complexes, with a special emphasis on those

dx.doi.org/10.1021/ic102237x |Inorg. Chem. 2011, 50, 6437–6448

Scheme 1. Filiation of the Six Manganese Compounds

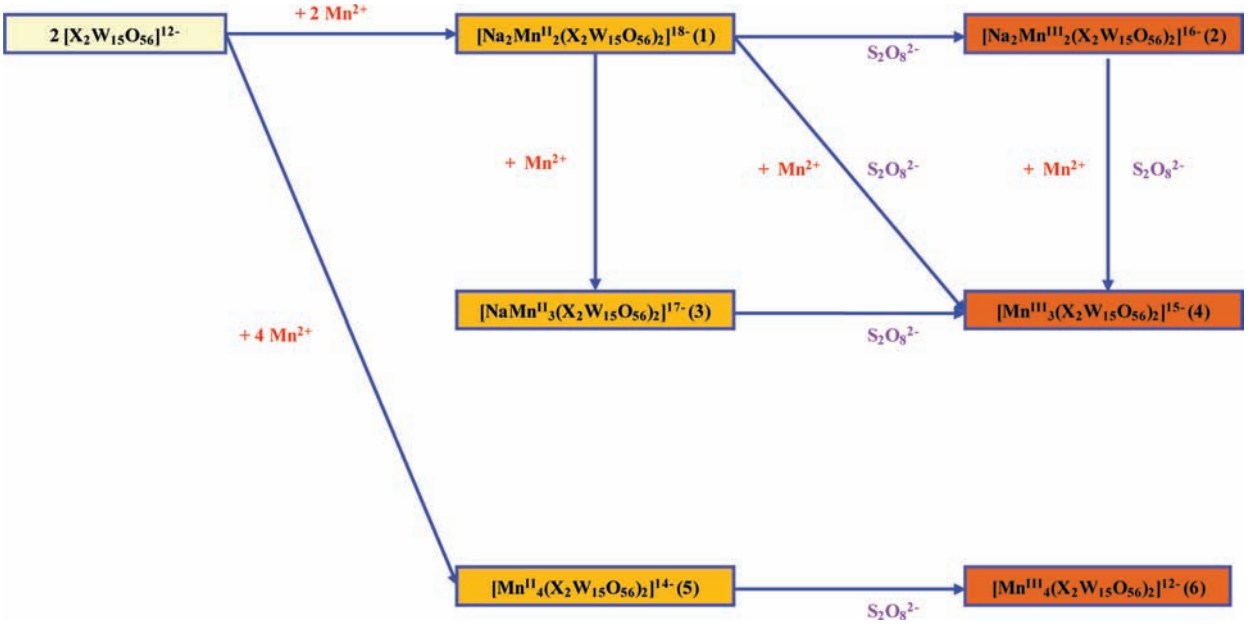

incorporating Mn^{3+} ions. To prepare **2**, a pure sample of **1** is dissolved in a molar solution of sodium chloride; $Na_2S_2O_8$ is used to oxidize the two Mn^{II} centers to Mn^{III}. The high Na^+ concentration that results from addition of an excess of $Na_2S_2O_8$ in the 1 M NaCl solution prevents the progression of **1** to **3** and then to **4**. As explained in previous studies,[3,10,20] disubstituted WDST structures are unstable in solution and evolve to more stable trisubstituted structures, which are known to be very stable in solution, even more so than the tetrasubstituted WDST structures. The progression of **1** to **3** is a structural rearrangement that proceeds by exclusion of a single Na^+ ion, an exclusion that cannot take place in the presence of an excess of sodium.

The synthesis of **3** starting from **1** is therefore less complicated as it corresponds to the final step of the rearrangement of **1** in solution. Although the WDST complexes containing four "d" metal centers are less stable than those with three centers, preparation of the later from the former is almost impossible and has never been described. Both configurations correspond to very stable states, and conversion of one to another is not trivial.

For the reasons mentioned above, the synthesis of **3**, from **1**, and the synthesis of **4**, from **1**, are straightforward and give very satisfactory yields (53%). However, two alternative methods were also attempted (see Supporting Information). Oxidation of a solution of **3** by $Na_2S_2O_8$ (alternative method 1) gives the highest yield, 83%. The preliminary step does however require the synthesis of **3** starting from **1** which proceeds with a 73% yield. Alternative method 2, starting from compound **2**, gives the lowest yield, 30%, with competitive formation of a fine black precipitate of MnO_2. Ultimately, both synthetic procedures lead to the same compound formally characterized by FTIR and electrochemistry. As expected, oxidation of **5** by $Na_2S_2O_8$ is done without any decomposition and led to a pure sample of **6**. Scheme 1 summarizes the synthesis of this family of manganese-containing Wells–Dawson sandwich-type complexes starting from the lacunary species $[X_2W_{15}O_{56}]^{12-}$ (where X = As or P).

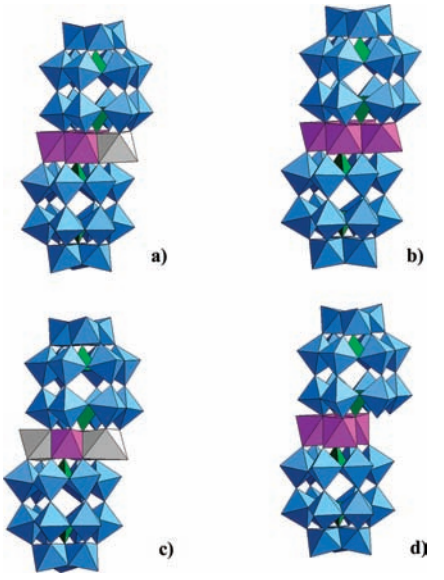

Figure 1. Polyhedral representations of (a) **3**, (b) **5**, (c) **2**, and (d) **4**: blue octahedra, WO_6; green tetrahedra, AsO_4; purple octahedra, MnO_6; gray octahedra, NaO_6.

Crystal Structure. As the crystal structure of **5** has already been reported[8m] and since it has not been possible to isolate single crystals of **1** and **6** of sufficient quality for X-ray characterization, only the structures of **2**, **3**, and **4** have been studied by single-crystal X-ray crystallography and will be compared to the previously characterized structure of **5**. The overall structure of the four anions in **2**, **3**, **4**, and **5** is similar (Figure 1). In these anions two $[As_2W_{15}O_{56}]^{12-}$ moieties sandwich a central unit, the composition of which differs from one anion to the other (Figure 2). In the four structures the modes of junction are $\alpha\beta\beta\alpha$,[21] as almost exclusively observed for Dawson sandwich-type structures, a consequence of their

dx.doi.org/10.1021/ic102237x |*Inorg. Chem.* 2011, 50, 6437–6448

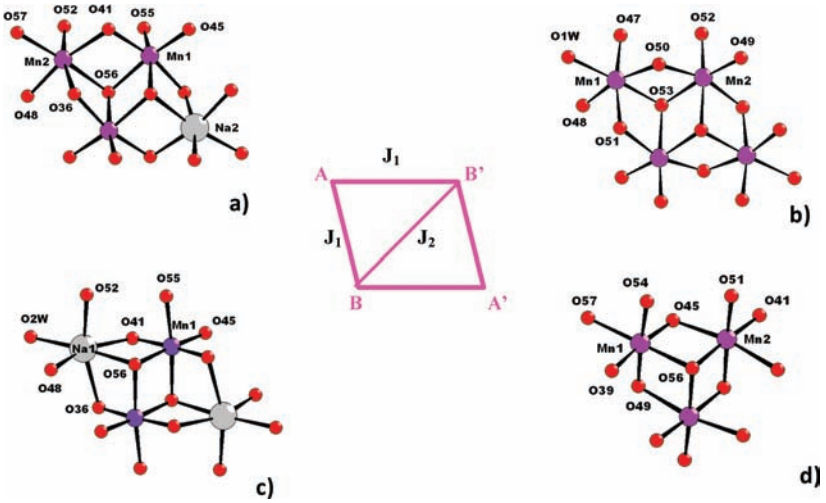

Figure 2. Schematic representation and atomic-labeling scheme of the rhombic central $\{M_4O_{14}(H_2O)_2\}$ unit in (a) **3**, (b) **5**, (c) **2**, and (d) **4**.

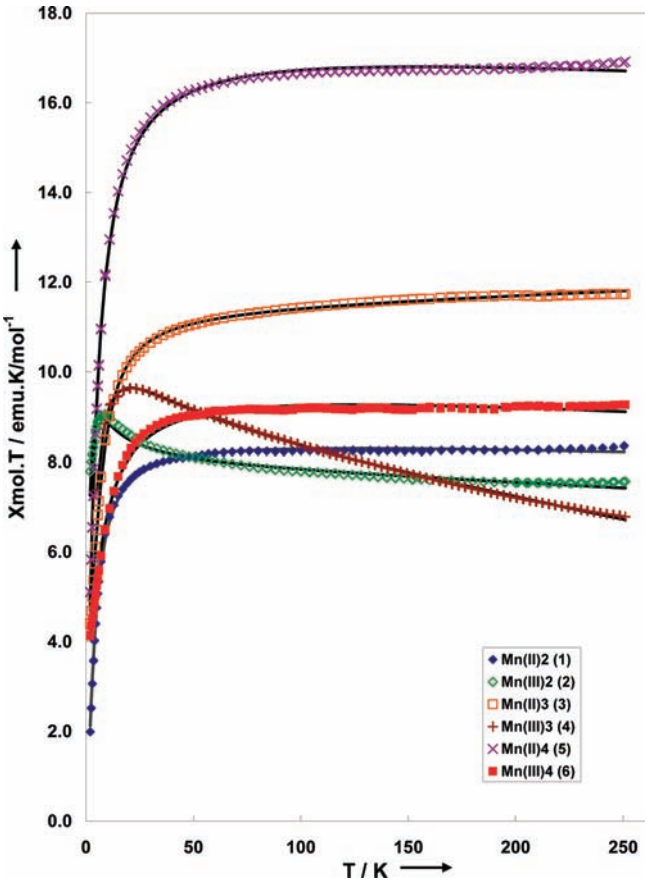

Figure 3. Plot of the $X_{mol}T$ product as a function of temperature for the Mn_xAs_4 compounds identified by the magnetic ions composing their central cluster. The symbols represent the experimental data and the continuous lines the least-squares fits using the parameters reported in Table 3.

greater stability.[8i] Only three exceptions have been encountered: the dinuclear αααα-$[Na_2(H_2O)_2Fe^{III}{}_2(P_2W_{15}O_{56})_2]^{16-}$ complex[8g] with two α junctions between the trivacant POMs and the central unit and the ααβα-$[Na(H_2O)Fe^{III}(H_2O)Fe^{III}{}_2(P_2W_{15}O_{56})_2]^{12-}$[8i] and ααβα-$[M^{II}(H_2O)Fe^{III}{}_2(P_2W_{15}O_{56})(P_2M^{II}{}_2(H_2O)_4W_{13}O_{52})]^{16-}$ (M = Cu, Co)[8h] POMs with dissymmetrical junctions. In **5**,[8m] the central unit is the rhombic tetranuclear $\{Mn_4O_{14}(H_2O)_2\}$ core in which the four metallic centers in octahedral coordination have the +II oxidation state, the two external ions (A and A′ positions) being connected to a water molecule. One external Mn ion is missing in the structure of **3** and **4**, with the missing Mn position occupied by a sodium ion in **3** and remaining unoccupied in **4**. A possible explanation for compound **4** could lie in the Jahn−Teller effect, as proposed by Anderson and Hill.[8i] This effect could prevent the accommodation of a sodium ion in the vacancy. Furthermore, the Jahn−Teller effect could explain the greater distortion of the Mn^{III} coordination sphere in **4** compared to Mn^{II} in **3** (Table 2).

In the structure of **2**, each of the two outer sites of the rhombic unit (A and A′ positions) is occupied by one sodium ion and the inner sites (B and B′ positions) by two Mn^{III} ions. In all the structures the oxidation states of the Mn ions have been confirmed by valence bond calculations[22] (Table 2) and by X-ray photoelectron spectroscopy (see Supporting Information). It should be noted that in the structures of **3** and **4** the central rhombic unit lies on an inversion center which induces a crystallographic disorder on the outer positions. More precisely, in **3** the A and A′ positions are occupied statistically by 50% Mn2 and 50% Na2, and in **4** these positions are occupied only by Mn1 with an occupancy factor of 0.5 (Figure 2). The A···A′ distance in the central rhombic unit increases in the following order: **4** < **5** < **3** < **2** (Table 2), in agreement with the fact that a disordered Mn ion within a vacant site has a smaller size than a Mn ion, which has an even smaller size than a sodium ion.

Magnetic Studies. The temperature dependence of the magnetization was studied in a 0.1 T field from 2 to 250 K. To confirm that no saturation of the magnetization takes place in these conditions, data were also collected in a 0.5 T field between 4.5 and 250 K. Due to a lower mass of the sample, only the higher field was suitable to record significant data for **4**. In order to reveal the specific behavior of each compound the value of the $X_{mol}T$ product, where X_{mol} is the molar susceptibility, was then calculated from the low-field experimental data and plotted as a function of temperature T in Figure 3. Except for **2** and **4**, the $X_{mol}T$ product increases monotonously with T. This behavior is a first indication

dx.doi.org/10.1021/ic102237x |*Inorg. Chem.* 2011, 50, 6437–6448

Table 3. Magnetic Parameters and First Energy Levels of the Compounds under Study

compound	1	2	3	4	5	6
g	1.987	2.298	1.867	1.973	2.005	1.815
J_1/cm^{-1}	0	0	−0.36	1.99	−0.18	−0.22
J_2/cm^{-1}	−0.30	0.59	0.40	−1.39	−0.14	−0.54
$X_0/emu.mol^{-1}$	-1.36×10^{-3}	-2.23×10^{-3}	1.78×10^{-3}	-9.12×10^{-3}	-2.55×10^{-3}	-2.46×10^{-3}
T_{CW}/K	0	−1.59	0	−3.52	0	0
E_0/cm^{-1} [S_T]	−5.25 [0]	−4.72 [4]	−16.95 [2.5]	−24.26 [4]	−9.05 [0]	−7.64 [2]
E_1/cm^{-1} [S_T]	−4.65 [1]	0 [3]	−13.28 [3.5]	−23.88 [5]	−8.69 [1]	−7.60 [3]

of the presence of antiferromagnatic interactions between the Mn ions in these compounds. Conversely, the particular shape observed for **2** and **4** is the maximum reached for the temperature close to 8 and 21 K, respectively. It reveals a ferromagnetic coupling of the oxygen-connected Mn^{III} ions and an antiferromagnetic coupling between neighboring clusters. For all the compositions the values of the $X_{mol}T$ product are nearly constant above 50 K; this contrasts strongly with the behavior observed for analogous iron clusters[23] and indicates that magnetic interactions are clearly weaker between Mn ions than between Fe ions. For **4**, the observed decrease of the $X_{mol}T$ product has an extrinsic origin as discussed in the next part.

To carry out a quantitative analysis of the magnetic interactions the experimental susceptibility of the complexes under study was written as

$$X_{mol} = [T/(T - T_{CW})X_{cluster}] + X_0$$

where T_{CW} is the negative Curie−Weiss temperature accounting for the mean field corrections associated to antiferromagnetic intercluster interactions, X_0 represents temperature-independent contributions, and $X_{cluster}$ represents the intrinsic susceptibility of the cluster. X_0 is mainly due to the diamagnetism of the ligands and of the sample holder but may also include some temperature-independent paramagnetic contribution. $X_{cluster}$ is given by the following equation

$$X_{cluster} = \frac{g^2 N\beta^2 \langle S_T(S_T + 1)\rangle}{3kT}$$

in which the mean value $\langle S_T(S_T + 1)\rangle$ depends on the temperature which determines the population of the energy levels resulting from the individual spin coupling. These energy levels are eigenvalues of the magnetic Hamiltonian of the cluster. For the polyanions under study, the more general Hamiltonian is that describing tetranuclear clusters; however, those related to trinuclear or dinuclear clusters may be easily deduced from it by setting to zero the spin value of one or two of the four ions.

As the magnetic ions of the tetranuclear clusters are found at the corners of an almost regular rhomboid, the magnetic interactions can be represented by two exchange constants, J_1 and J_2, describing, respectively, the interactions along the sides of the rhomboid and that along its shortest diagonal. Taking into account this particular geometry, the magnetic energy of the cluster can be described by the following Heisenberg-type Hamiltonian

$$\hat{H} = -2J_1(\hat{S}_1\hat{S}_2 + \hat{S}_2\hat{S}_3 + \hat{S}_3\hat{S}_4 + \hat{S}_4\hat{S}_1) - 2J_2\hat{S}_1\hat{S}_3$$

The eigenvalues of this Hamiltonian operator are obtained by the vector-coupling method of Kambe[24]

$$E_i(S_T, S_{13}, S_{24}) = -J_1[S_T(S_T + 1) - S_{13}(S_{13} + 1) - S_{24}(S_{24} + 1)] - J_2[S_{13}(S_{13} + 1) - S_1(S_1 + 1) - S_3(S_3 + 1)]$$

where S_{13}, S_{24}, and S_T are eigenvalues of the spin operators $\hat{S}_{13} = \hat{S}_1 + \hat{S}_3$, $\hat{S}_{24} = \hat{S}_2 + \hat{S}_4$, and $\hat{S}_T = \hat{S}_{13} + \hat{S}_{24}$.

The number of magnetic states of energy E_i described by the (S_T, S_{13}, S_{24}) combinations depends on the number of magnetic ions in the cluster and of their spins. This number of states ranges from 5 for the **2** cluster to 146 for the **5** cluster.

After calculation of the energies E_i, the mean value of $\langle S_T(S_T + 1)\rangle$ is obtained as

$$\langle S_T(S_T + 1)\rangle = \sum a_i \exp(-E_i/kT)/\sum b_i \exp(-E_i/kT)$$

with $b_i = 2S_T(E_i) + 1$ and $a_i = b_i S_T(E_i)(S_T(E_i) + 1)$.

These formulas made it possible to simulate a $X_{mol}T$ curve as a function of T from a given set of physical parameters. From the best simulation, fitting the calculated $X_{mol}T$ values to the experimental ones, it is possible to determine the magnetic parameters describing the cluster (Table 3). To obtain these parameters, a FORTRAN program was written using the MINUIT minimization routine developed in CERN. The Landé g factors are close to 2 for all samples; the deviations from this value may be due to experimental uncertainties such as the exact molar weights of the compounds which depend on their water contents.

The values of the J_1 and J_2 parameters are rather weak and of the same order as those reported for the $[Mn^{II}_2(H_2O)_2\text{-}Mn^{II}_2(P_2W_{15}O_{56})_2]^{16-}$,[8e] whereas quite larger values were determined for Fe^{III}−Fe^{III} or Fe^{III}−Mn^{II} interactions.[23] Moreover, there is no simple correlation between, on the one hand, the signs of the J_1 and J_2 parameters and, on the other hand, the valence of the manganese ions or the number of manganese ions in the cluster. It is worth noting here that both J_1 and J_2 describe interactions which are the sum of three contributions: two of them are of the superexchange type; they are mediated by two bridging oxygen ions forming the edge shared by two neighboring MnO_6 octahedra, while the third is a direct interaction between two close Mn ions. Therefore, some competition between ferromagnetic and antiferromagnetic interactions depending strongly on the geometry of the cluster is expected.

When the interactions along the shortest diagonal of the rhomboid are antiferromagnetic the difference in energy $(E_1 - E_0)$ between the ground state and the first excited state is lower than 1 cm^{-1}, whereas it was close to 4 cm^{-1} when J_2 described a ferromagnetic interaction. Therefore, the presence of a ferromagnetic interaction stabilizes the ground state. In the case of the **3** cluster, this stabilization is associated with a spin configuration which can simultaneously satisfy all the interactions: the spins of the two Mn ions located on the B and B′ positions are parallel, whereas the spin of the third ion is antiparallel to them. Such a stabilization does not exist for a cluster containing more than two magnetic ions when J_2 is negative whatever the sign of J_1. The result of the competition between antagonist interactions depends on the relative strengths of the interactions described by J_1 and J_2

dx.doi.org/10.1021/ic102237x |Inorg. Chem. 2011, 50, 6437–6448

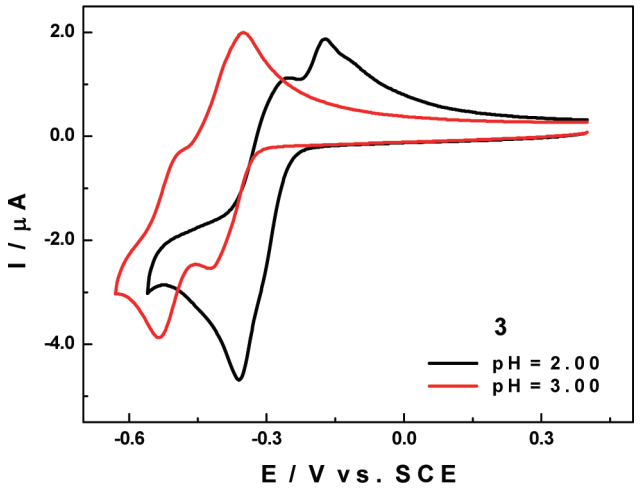

Figure 4. Cyclic voltammograms of **3** at pH 2 (black line) and pH 3 (red line) in 0.2 M Na_2SO_4 + H_2SO_4; POM concentration 0.2 mM. Scans are restricted to the first two reduction waves of tungsten. Scan rate 10 mV s^{-1}; reference electrode SCE.

as revealed by the parameters describing the tetranuclear clusters. In **5** the interactions along the sides of the rhomboid are the strongest; consequently, the spins of the Mn ions located on subsequent corners are antiparallel in the ground state which has a total spin equal to 0. Conversely, in **6** the interaction along the shortest diagonal is the strongest but in competition with four interactions along the sides. The result of this competition is a ground state with a total spin equal to 3, which represents some compromise for the spin configuration.

Except for **4**, the values of the temperature-independent susceptibilities X_0 are negative and may be associated with the diamagnetic character of the ligands and of the sample holder. For **4**, the contribution of the sample holder explains the high absolute value of X_0 since the mass of the sample under study was particularly small, as previously mentioned. The positive value of X_0 found for **3** may indicate that this compound exhibits an intrinsic temperature-independent paramagnetism. However, some experimental artifact cannot be discarded. Finally, Curie−Weiss temperatures T_{CW} were determined for compounds having a ground state with a total spin S_T different from zero. They have rather weak values in good agreement with the dipolar character of the intercluster interactions.

Stability and Electrochemistry Studies. UV−vis spectra were recorded on 2×10^{-5} M solutions of each of the compounds mentioned above as a function of pH over a period of 24 h. The stability criterion was reproducibility of spectra with respect to absorbance and wavelengths during this period of time. All complexes were found to be stable in solution over the pH range of 1−6. The spectra recorded at pH 1 and 6 are shown in the Supporting Information. Corroboration of stability was obtained by electrochemistry; cyclic voltammograms (CV) of the given compounds were reproducible after several hours.

We will first describe and discuss redox processes associated with the reduction of the tungsten framework on these sandwich-type complexes. Figure 4 shows the CVs of **3** at pH 2 and 3, restricted to the first tungsten waves and recorded at a scan rate of 10 mV s^{-1}. The CV patterns obtained in these media are typical of WDST complexes. At pH 2, this CV is composed of a main reduction wave located at −0.36 V vs SCE, with a more or less pronounced shoulder at −0.30 V. At pH 3 (CV in red in Figure 4), reduction potentials shift at higher pH values, resulting in a better pattern with greater separation between these two waves (pH 2, ΔE_{W1-W2} = 60 mV; pH 3, ΔE_{W1-W2} = 110 mV). The five other complexes show exactly the same behavior; their CVs are identical, and differences observed in the peak reduction potential values are too small to be taken into consideration (see Table 4 and Figures SI-9−SI-14, Supporting Information). Thus, considering only the W waves, we can conclude that at pH 2 and 3 (0.2 M Na_2SO_4 + H_2SO_4) Mn-containing WDST complexes present exactly the same electrochemical behavior, independent of the number or oxidation state of the manganese centers. This high degree of similarity in their electrochemical properties necessitates either of the two following conclusions: (1) electrical charges of these species have no or only a negligible influence on their redox potentials in these media; (2) there is preprotonation and/or ion-pair formation that brings the electrical charge of each complex to about the same value; consequently, their reducibilities will be similar. In fact, at a higher pH value (pH 6), where the proton concentration is too low to induce any preprotonation, the CVs of **1** and **5**, for example, differ more than they do at pH 2 or 3 (see Figures SI.1 and SI.2 and comments that follow, Supporting Information).

Table 4. Peak Reduction Potentials for the First Two Reduction Steps at pH 2 and 3 (0.2 M Na_2SO_4 + H_2SO_4) for Compounds 1, 3, 5, 2, 4 and 6[a]

	pH 2		pH 3	
	E_{pc1}/V	E_{pc2}/V	E_{pc1}/V	E_{pc2}/V
1	−0.300	−0.356	−0.424	−0.530
3	−0.300	−0.360	−0.422	−0.534
5	−0.310	−0.362	−0.422	−0.536
2	−0.308	−0.362	−0.426	−0.530
4	−0.306	−0.360	−0.421	−0.529
6	−0.296	−0.362	−0.421	−0.529

[a] CVs were recorded at a scan rate of 10 mV s^{-1}; working electrode glassy carbon. Potentials are quoted against SCE reference electrode.

Redox Behavior of the Manganese Centers. Redox processes associated with the manganese centers incorporated in each of these 6 complexes deserve special attention as the number and oxidation states of the manganese cations differ from one complex to another.

Mn^{II} Centers incorporated in 1, 3, and 5. As expected, oxidation of Mn^{II} ions within these three complexes is always easier at pH 3 than at pH 2 despite any differences in the number (2−4) or position (inner or/and outer sites) of the Mn centers. Consequently, the redox processes assigned to Mn^{II} centers in each case are better defined at pH 3 than at pH 2 (Figure SI-3, Supporting Information). Comparisons are therefore made at pH 3. In Figure 5 below, CVs of **1** and **3** are presented (the scan is restricted to Mn^{IV}/Mn^{II} redox processes). Mn^{II} oxidation clearly proceeds into two steps: (1) a slow electron transfer step that occurs between +0.55 and 1.05 V for both complexes and can be easily assigned to the Mn^{II}/Mn^{III} oxidation step; (2) the second electron transfer, assigned to the Mn^{III}/Mn^{IV} oxidation step, remains slow and is difficult to detect for complex **1**, while for **3** we observed a fast electron transfer characterized by a sharp wave with a peak at +1.17 V. On the other hand, reduction of these electrochemically generated Mn^{IV} species seems to proceed in a

dx.doi.org/10.1021/ic102237x |*Inorg. Chem.* 2011, 50, 6437–6448

single step, Mn^{IV}/Mn^{II} for both complexes, but with a smaller current for **1** as compared to **3** and **5**.

Differences observed here in the electrochemical behavior of these complexes can not only be related to the number of Mn^{II} centers contained in each complex (two for **1**, three for **3**, and four for **5**); we must also take into account their relative positions. The two Mn^{II} of **1**, located in inner sites, appear to be less accessible than those located in outer sites (compounds **3** and **5**). Therefore, when oxidized to a + IV state, they are less likely to form manganese oxides species which could be adsorbed onto the working electrode surface and redissolved (at least partly) during the reversed reduction. In comparison, for the additional Mn^{II} centers present in complexes **3** and **5**, in addition to being located in the outer sites, they are also each bonded to a water molecule (see Crystallographic structure section). Thus, they are much more likely to form oxide films on the working electrode surface when oxidized to a +IV state. In fact, in the CVs of **1**, **3**, and **5** presented in Figure 5 or Figure SI-17C, Supporting Information, the waves attributed to the Mn^{II}/Mn^{IV} redox steps have the characteristic "sharp-shape" of adsorption−desorption processes. Definitely it appears that a manganese oxide film is formed on the working electrode surface when one goes up to the +IV oxidation state; this film is almost completely desorbed during the backward scan in the reduction step back to the +II oxidation state. Another observation that highlights the differences between Mn centers located on the inner sites and those located on the outer sites is the evolution of a reduction peak current, I_{pc}, associated with the reduction process Mn^{IV}/Mn^{II}, with the number of Mn centers. Hypothetically, where there are 4 equivalent sites, we expect I_{pc} to be a linear function of the number of Mn centers present in each compound. Instead, I_{pc} increases exponentially when moving from complex **1**, with no "external" Mn^{II}, to **3**, and again to **5**, which contain one and two external Mn^{II}, respectively (see Figure SI-18, Supporting Information).

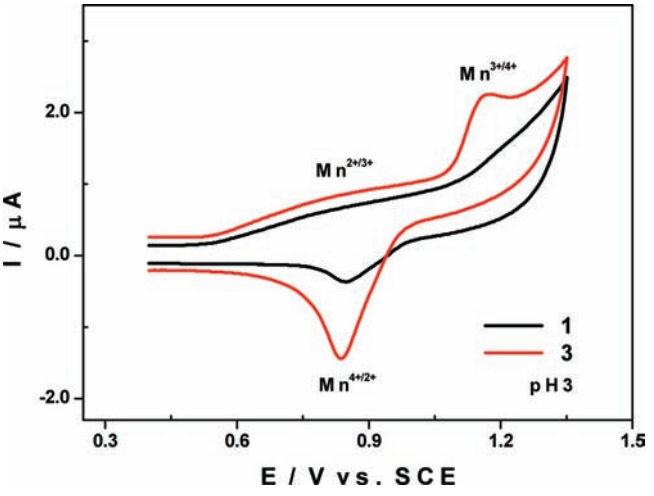

Figure 5. Cyclic voltammograms of **1** (black line) and **3** (red line) at pH 3 (0.2 M Na_2SO_4 + H_2SO_4); POM concentration = 0.2 mM. Scans are restricted to the redox processes attributed to Mn^{II} centers. Scan rate 10 mV s^{-1}; reference electrode SCE.

The potential scanning direction does not seem to have any influence on the location of the manganese peaks as observed on the CV of **5**, presented in Figure 6A. In fact, the first CV (black line) was completed as follows: potentials are first scanned in the negative direction down to −0.3 V vs SCE (at the bottom of the first W reduction) before going back in the direction of positive values up to 1.25 V vs SCE. The second CV (red line) was obtained by scanning in the opposite direction. The position of the Mn redox waves are located at exactly the same potential values (E_{pa} = 1.07 V and E_{pc} = 0.82 V) independently of the direction in which the scan was done. E_{pa}, E_{pc}, and I_{pa} (oxidation current) remained unchanged over successive cycles, while I_{pc} (reduction current) linearly increased. We can conclude that the Mn oxides adsorbed on the working electrode surface during the oxidation step are not completely redissolved during the consecutive reduction step. This results in an increase, albeit small but gradual, in the thickness of this film over successive cycles, hence the increase in I_{pc} which corresponds to its redissolution. This film seems not to cause a significant modification of the working electrode (E_{pa} and I_{pa} are almost invariant, Figure SI-19, Supporting Information). Interestingly, after restricting the

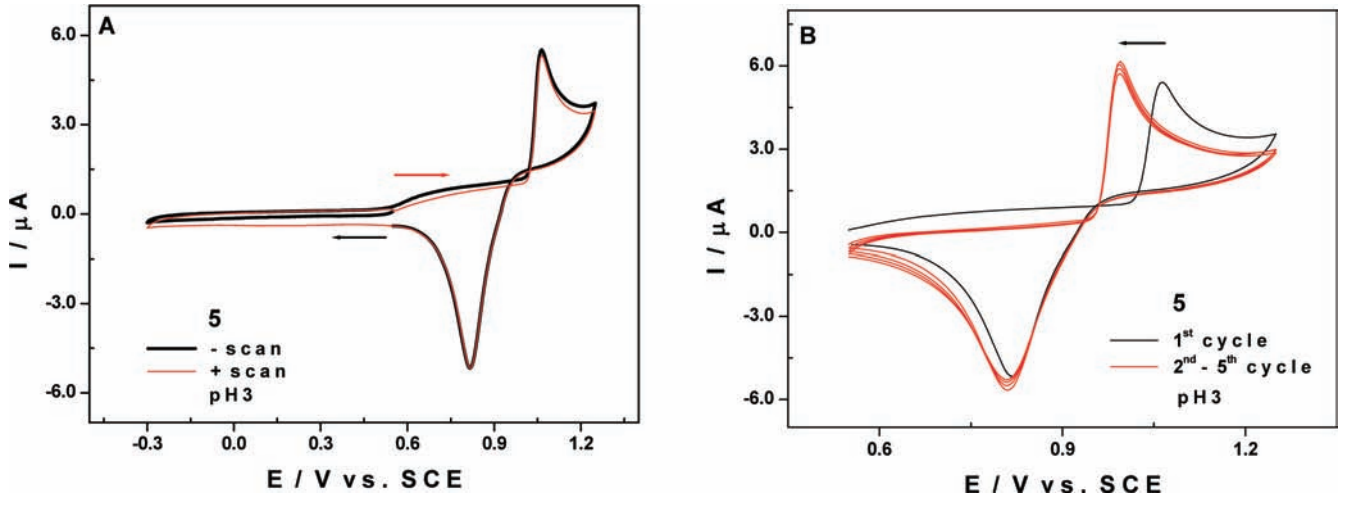

Figure 6. Cyclic voltammograms of **5** at pH 3(0.2 M Na_2SO_4 + H_2SO_4); POM concentration 0.2 mM. Scan rate 10 mV s^{-1}; reference electrode SCE. (A) Potentials were initially scanned down to −0.3 V and then up to +1.25 V for the first experiment (black line); for the second experiment the potentials were initially scanned up to +1.25 V and then down to −0.3 V. (B) Potentials were scanned between +0.55 and +1.25 V; the first cycle is in black and the following in red.

dx.doi.org/10.1021/ic102237x |*Inorg. Chem.* 2011, 50, 6437–6448

cycling within the interval [0.55 V; 1.25 V] (Figure 6B) a slight increase in I_{pc} over successive cycles is still observed, while E_{pc} remained almost constant. Meanwhile, between the first and the second cycle, E_{pa} shifted by about 80 mV in the direction of negative potentials with no subsequent shifting in any of the following cycles. As observed for I_{pc}, there was a slight and gradual increase of I_{pa}. Regarding the behavior of the reduction wave, the conclusion drawn above is still valid, i.e., a gradual increase of the thickness of the Mn oxide film leads to an increase of I_{pc}. However, the nature of this oxide film seems to be different as the behavior of the working electrode is significantly modified during the subsequent cycle which made the oxidation of Mn easier (ΔE = +0.07 V). In other words, scanning the potential down to −0.3 V is necessary but may be not sufficient to regenerate an active working electrode surface and minimize changes of Mn waves during cycling (potentials and currents). If the scanning is stopped before this limit (at +0.55 V, for example), this significantly modifies the working electrode surface, altering its reactivity toward oxidation of Mn^{II} centers. In fact, exploration of potential up to the $Mn^{II/IV}$ redox wave always irreversibly modifies the working electrode surface, and a full polishing procedure[17] is required if one wants to recover its initial activity and collect reliable data.

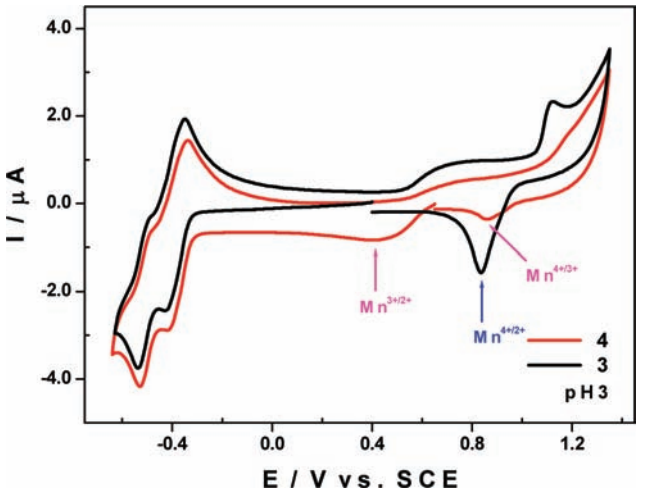

Figure 7. Comparison of CVs of **3** (black line) and **4** (red line) at pH 3 (0.2 M Na_2SO_4 + H_2SO_4). POM concentration: 0.2 mM. Scan rate: 10 mV s^{-1}. Reference electrode: SCE.

Specific Behaviors of Mn^{III} Centers Incorporated in 2, 4, and 6. As stated previously, we synthesized and characterized for the first time WDST complexes that contain Mn^{III} centers. For this reason, particular attention will be given to their pioneering electrochemical characterization. Figure 7 below shows the CVs of **3** (black line) and **4** (red line) recorded at pH 3 (0.2 M Na_2SO_4 + H_2SO_4) and summarizes typical electrochemical behaviors that differentiate Mn^{III} complexes from the Mn^{II} complexes. As can be seen, the presence of Mn^{III} ions within the structure of compound **4** leads to the emergence of a new wave located between +0.55 and +0.40 V that does not exist in the CV of **3**. A similar observation is apparent in the CVs of **2** and **6** compared to the CVs of **1** and **5**, respectively. This new wave is obviously attributed to the reduction Mn^{III}/Mn^{II}. Another observation that deserves special attention is the change in the shape of the wave associated with oxidation of the manganese(II) species that is electrochemically generated during forward scan (reduction steps). We still have a two-step process, Mn^{II}/Mn^{III} followed by Mn^{III}/Mn^{IV}, but in comparison with the CV of **3** this process has clearly become more difficult in the case of WDST containing Mn^{III} (average potential shift of about 70 mV in the direction of more positive potentials and drop of oxidation currents). Another surprising behavior that distinguishes these two families of complexes is that for the Mn^{III}-containing WDST complexes (**2**, **4**, and **6**) the reduction of the electrochemically generated Mn^{IV} species still undergoes two steps, Mn^{IV}/Mn^{III} and Mn^{III}/Mn^{II}, contrary to what is observed with the Mn^{II}-containing WDST complexes (**1**, **3**, and **5**).

Now that the main differences that distinguished the Mn^{III} complexes from those with Mn^{II} have been highlighted, we can discuss in greater detail the electrochemical properties that characterize these new Mn^{III} complexes. First, pH influence is less pronounced for Mn^{III}/Mn^{II} reduction than it is for reduction of the W framework. For complex **4**, for example, this wave only shifts about 80 mV when moving from pH 2 to pH 3, while the

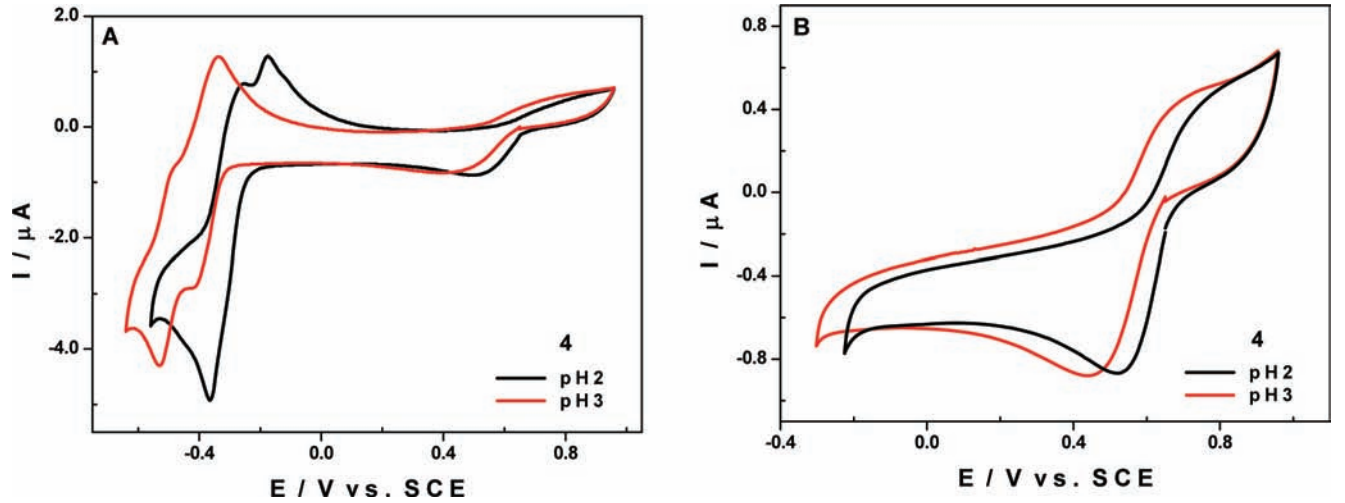

Figure 8. Cyclic voltammograms of **4** in 0.2 M Na_2SO_4 + H_2SO_4, pH 2 (black line) and pH 3 (red line); POM concentration 0.2 mM. Scan rate 10 mV s^{-1}; reference electrode SCE. (A) Scans were initially in the direction of negative potential (W redox waves) and then back toward a positive potential of +0.96 V (Mn redox wave). (B) Potential scans were restricted between −0.30 and +0.96 V to highlight the $Mn^{III/II}$ redox process.

dx.doi.org/10.1021/ic102237x |*Inorg. Chem.* 2011, 50, 6437–6448

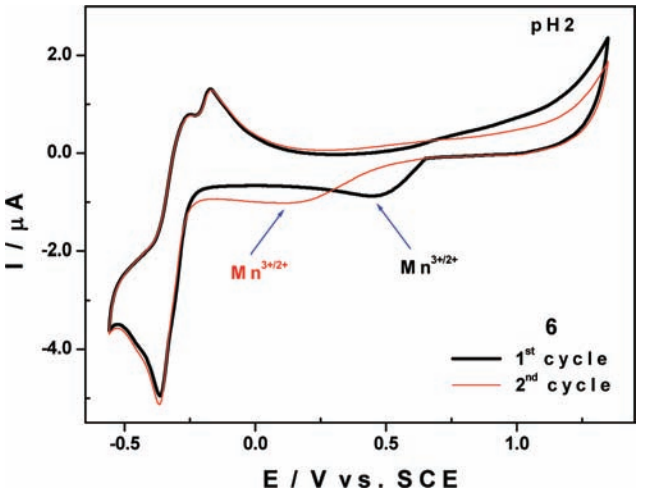

Figure 9. Successive cyclic voltammograms of **6** in 0.2 M Na_2SO_4 + H_2SO_4, pH 2. First cycle, black line; second cycle, red line. POM concentration 0.2 mM. Initial potential, +0.65 V. Initial potential scanning direction: negative. Scan rate 10 mV s^{-1}; reference electrode SCE.

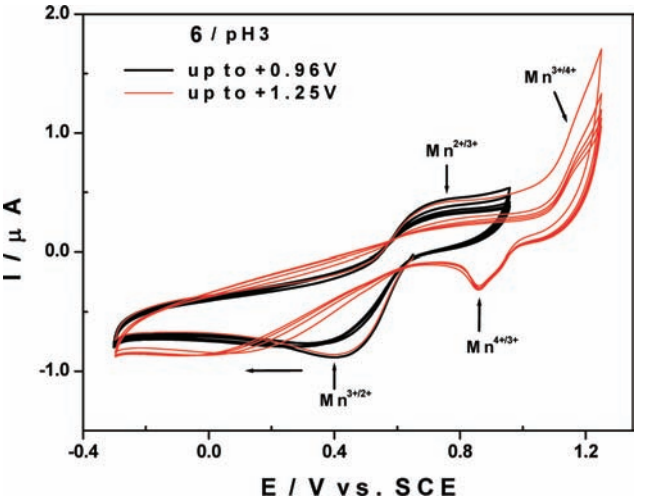

Figure 10. Successive cyclic voltammograms of **6** in 0.2 M Na_2SO_4 + H_2SO_4 at pH 3. Black lines: potential scan is restricted between −0.30 and +0.96 V where only the $Mn^{III/II}$ redox process is observed (black line). Potential scan is extended up to +1.25 V to achieve oxidation of Mn centers up +IV and highlight the influence of the CV pattern (red line). POM concentration 0.2 mM. Initial potential, +0.65 V. Initial potential scanning direction: negative. Scan rate 10 mV s^{-1}; reference electrode SCE.

first and second W reduction waves shift 115 and 170 mV, respectively (see Figure 8). Exactly the same behavior is observed for compounds **2** and **6** with roughly the same values for the shifts in redox potential.

Further discussion on the electrochemical properties of these Mn^{III} complexes will be illustrated by observations made with compound **6**. This compound has the advantage of containing four Mn^{III} centers, with two located on outer sites, resulting in a magnification of their redox properties. The CV of **6** recorded
at pH 2 is shown in Figure 9; potentials are scanned from +0.65 V down to −0.56 V (i.e., after the first tungsten reduction steps) and then up to +1.35 V (i.e., after oxidation of the manganese centers) and, finally, back to +0.65 V. This cycle was repeated twice. During the first cycle, the wave attributed to reduction of Mn^{III}/Mn^{II} appeared at +0.45 V; this wave shifted down to +0.10 V during the second cycle, while the tungsten redox waves are superimposed over the two cycles. It appears that oxidation of Mn^{II}, electrochemically generated during reduction steps, significantly modifies the working electrode surface during the first cycle and alters its reactivity; Mn^{III} reduction therefore becomes more difficult during the second cycle (ΔE = −350 mV). However, as discussed previously for compounds **1**, **3**, and **5**, a scan of potentials down to −0.20 V in this medium (0.2 M Na_2SO_4 + H_2SO_4/pH 2) is sufficient for satisfactory regeneration of the working electrode surface, and the tungsten redox waves are then reproducible over successive cycles.

Oxidation of the Mn^{II} centers, electrochemically generated during the negative scan, and subsequent reduction of the new Mn^{IV} species are barely detectable at pH 2, while for complex **5**, which contains exactly the same number of Mn centers, very well-defined redox waves are observed (see Figure SI-17C, Supporting Information). However, cycling between −0.225 and +1.35 V finally produces a small bump around +1.0 V, which is evidence of the oxidation of these Mn^{II} species (with deposition of manganese oxides on the working electrode surface) and their reduction (with redissolution of adsorbed manganese oxides, see Figure SI-21, Supporting Information.

At pH 3 the phenomenon that was barely detectable at pH 2 becomes more visible (Figure 10). Mn^{II} oxidation clearly appears as a two-step process with Mn^{II}/Mn^{III} oxidation, as the first step, located around +0.70 V followed by Mn^{III}/Mn^{IV} oxidation, the second step, at around +1.16 V. The associated reduction also proceeds as a two-step process; the first step Mn^{IV}/Mn^{III} reduction at +0.86 V and the second step Mn^{III}/Mn^{II} reduction had a peak potential that evolved over successive scans. Indeed, during the first cycle (when the potential scan is done in the negative potential direction starting from +0.65 V) direct reduction of Mn^{III} centers within the molecule of **6** occurs at +0.40 V. During the following cycles, reduction of the electrochemically regenerated Mn^{III} species becomes more difficult (+0.20 V instead of +0.40 V) for reasons we mentioned above (modification of the working electrode by deposition of manganese oxides). When the cycling is restricted between −0.3 and +0.96 V, the Mn^{III}/Mn^{II} redox wave barely moves over successive scans. A slight decrease of the reduction current, in part due to the derivation of the baseline, is observed (CVs in black in Figure 10). Here, again, as observed above at pH 2, it is possible to isolate the redox couple $Mn^{III/II}$ without any trace of Mn^{IV} which will pollute the electrode.

Ultimately it appears that redox behaviors associated with Mn^{III} centers within **2**, **4**, and **6** are quite different from the one observed with Mn^{II} in complexes **1**, **3**, and **5**. For example, with the Mn^{II} complexes it was not possible to observe separately the Mn^{III}/Mn^{II} reduction step. In contrast, it was easier to reach manganese higher oxidation states (+V) with Mn^{II} complexes than with their Mn^{III} counterparts (see Figure SI-23, Supporting Information). In a previous study, Keita et al. have shown that it was possible to easily form Mn^{V} species starting from the Keggin sandwich-type complex $[Mn^{III}(H_2O)_3(Sb_2W_9O_{33})_2]^{9-}$.[11e] In the present case, Mn^{III} centers within WDST seem to be less oxidizable than Mn^{II} centers.

dx.doi.org/10.1021/ic102237x |*Inorg. Chem.* 2011, 50, 6437–6448

CONCLUSIONS

We prepared three unprecedented Mn^{III}-containing WDST complexes, $[Na_2(H_2O)_2Mn^{III}{}_2(As_2W_{15}O_{56})_2]^{16-}$ (**2**), $[Mn^{III}(H_2O)Mn^{III}{}_2(As_2W_{15}O_{56})_2]^{15-}$ (**4**), and $[Mn^{III}{}_2(H_2O)_2Mn^{III}{}_2(As_2W_{15}O_{56})_2]^{12-}$ (**6**). Their parent Mn^{II} analogues, $[Na_2(H_2O)_2Mn^{II}{}_2(As_2W_{15}O_{56})_2]^{18-}$ (**1**) and $[Na(H_2O)_2Mn^{II}(H_2O)Mn^{II}{}_2(As_2W_{15}O_{56})_2]^{17-}$ (**3**), are also novel. These five new complexes were fully characterized by FTIR, ATG, UV−vis, elemental analysis, magnetic susceptibility, electrochemistry, and single-crystal X-ray crystallography, where possible. Comparable studies carried out on both Mn^{II} complexes and their well-known parent $[Mn^{II}{}_2(H_2O)_2Mn^{II}{}_2(As_2W_{15}O_{56})_2]^{16-}$ (**5**) clearly demonstrate the influence of the oxidation states of the Mn centers (+II or +III) on their structural, magnetic, and electrochemical properties. We isolated, using cyclic voltammetry, the redox couple $Mn^{III/II}$. We also observed that it was easier to reach the higher oxidation states of manganese (+IV and +V) starting with the Mn^{II}-containing WDST complexes than with their Mn^{III} counterparts. Possibilities of preparing mixed-metal WDST complexes with Mn^{III} and other d or f metal ions such as Fe^{III}, Cr^{III}, or Gd^{III} promise very interesting magnetic properties.

ASSOCIATED CONTENT

Supporting Information. Three X-ray crystallographic files in CIF format of $[Na_2(H_2O)_2Mn^{III}{}_2(As_2W_{15}O_{56})_2]^{16-}$, $[Mn^{III}(H_2O)Mn^{III}{}_2(As_2W_{15}O_{56})_2]^{15-}$, and $[Na(H_2O)_2Mn^{II}(H_2O)Mn^{II}{}_2(As_2W_{15}O_{56})_2]^{17-}$; two alternative methods for the synthesis of compound **4**; X-ray photoelectron spectroscopy results; UV−vis spectra and CVs that support the stability of the 6 compounds in solution from pH 1 to pH 6; complementary electrochemical characterization of all the polyoxometalates studied in this work and TGA results. This material is available free of charge via the Internet at http://pubs.acs.org.

AUTHOR INFORMATION

Corresponding Author

*E-mail: israel.mbomekalle@chimie.uvsq.fr.

ACKNOWLEDGMENT

This work was supported by the Centre National de la Recherche Scientifique (UMR 8180 and 8182), the University of Versailles, and the University of Paris-Sud XI.

REFERENCES

(1) Contant, R.; Hervé, G. *Rev. Inorg. Chem.* **2002**, *22*, 63–111.
(2) Long, D.-L.; Tsunashima, R.; Cronin, L. *Angew. Chem., Int. Ed.* **2010**, *49*, 1736–1758.
(3) Hill, C. L., Guest Ed. *Chem. Rev.* **1998**, *98*, 1−389.
(4) Keita, B.; Nadjo, L. *J. Mol. Catal. A* **2007**, *262*, 190–215.
(5) Long, D. -L.; Burkholder, E.; Cronin, L. *Chem. Soc. Rev.* **2007**, *36*, 105–121.
(6) Kortz, U.; Müller, A.; Slageren, J.v.; Schnack, J.; Dalal, N. S.; Dressel, M. *Coord. Chem. Rev.* **2009**, *253*, 2315–2327.
(7) Keita, B.; Liu, T.; Nadjo, L. *J. Mater. Chem.* **2009**, *19*, 19–33.
(8) (a) Finke, R. G.; Droege, M. W. *Inorg. Chem.* **1983**, *22*, 1006–1008. (b) Finke, R. G.; Droege, M. W.; Domaille, P. J. *Inorg. Chem.* **1987**, *26*, 3886–3896. (c) Weakley, T. J. R.; Finke, R. G. *Inorg. Chem.* **1990**, *29*, 1235–1241. (d) Finke, R. G.; Weakley, T. J. R. *J. Chem. Crystallogr.* **1994**, *24*, 123–128. (e) Gómez-García, C. J.; Borrás-Almenar, J. J.; Coronado, E.; Ouahab, L. *Inorg. Chem.* **1994**, *33*, 4016–4022. (f) Bi, L. H.; Wang, E.-B.; Peng, J.; Huang, R. D.; Xu, L.; Hu, C. W. *Inorg. Chem.* **2000**, *39*, 671–679. (g) Zhang, X.; Anderson, T. M.; Chen, Q.; Hill, C. L. *Inorg. Chem.* **2001**, *40*, 418–419. (h) Anderson, T. M.; Hardcastle, K. I.; Okun, N.; Hill, C. L. *Inorg. Chem.* **2001**, *40*, 6418–6425. (i) Anderson, T. M; Zhang, X.; Hardcastle, K. I.; Hill, C. L. *Inorg. Chem.* **2002**, *41*, 2477–2488. (j) Ruhlmann, L.; Nadjo, L.; Canny, J.; Contant, R.; Thouvenot, R. *Eur. J. Inorg. Chem.* **2002**, 975–986. (k) Ruhlmann, L.; Canny, J.; Contant, R.; Thouvenot, R. *Inorg. Chem.* **2002**, *41*, 3811–3819. (l) Mbomekalle, I. M.; Keita, B.; Nadjo, L.; Berthet, P.; Hardcastle, K. I.; Hill, C. L.; Anderson, T. M. *Inorg. Chem.* **2003**, *42*, 1163–1169. (m) Mbomekalle, I. M.; Keita, B.; Nadjo, L.; Berthet, P.; Neiwert, W. A.; Hill, C. L.; Ritorto, M. D.; Anderson, T. M. *Dalton Trans.* **2003**, *13*, 2646–2650. (n) Mbomekalle, I. M.; Keita, B.; Nadjo, L.; Berthet, P.; Hardcastle, K. I.; Hill, C. L.; Anderson, T. M. *Inorg. Chem.* **2003**, *42*, 1163–1169. (o) Mbomekalle, I. M.; Keita, B.; Nadjo, L.; Neiwert, W. A.; Zhang, L.; Hardcastle, K. I.; Hill, C. L.; Anderson, T. M. *Eur. J. Inorg. Chem.* **2003**, 3924–3928. (p) Ruhlmann, L.; Canny, J.; Vaissermann, J.; Thouvenot, R. *Dalton Trans.* **2004**, 794–800. (q) Fang, X.; Anderson, T. M.; Benelli, C.; Hill, C. L. *Chem.—Eur. J.* **2005**, *11*, 712–718. (r) Hussain, F.; Reicke, M.; Janowski, V.; de Silva, S.; Futuwi, J.; Kortz, U *C. R. Chim.* **2005**, *8*, 1045–1056. (s) Mbomekalle, I. M.; Cao, R.; Hardcastle, K. I.; Hill, C. L.; Ammam, M.; Keita, B.; Nadjo, L.; Anderson, T. M. *C. R. Chim.* **2005**, *8*, 1077–1086. (t) Anderson, T. M.; Fang, X.; Mbomekalle, I. M.; Keita, B.; Nadjo, L.; Hardcastle, K. I.; Farsidjani, A.; Hill, C. L. *J. Cluster Sci.* **2006**, *17*, 183–195. (u) Ruhlmann, L.; Costa-Coquelard, C.; Canny, J.; Thouvenot, R. *Eur. J. Inorg. Chem.* **2007**, 1493–1500. (v) Ruhlmann, L.; Costa-Coquelard, C.; Canny, J.; Thouvenot, R. *J. Electroanal. Chem.* **2007**, *603*, 260–268. (w) Pradeep, C. P.; Long, D.-L.; Koegerler, P.; Cronin, L. *Chem. Commun.* **2007**, *41*, 4254–4256. (x) Fang, X.; Koegerler, P. *Chem. Commun.* **2008**, *29*, 3396–3398.
(9) (a) Hill, C. L.; Prosser-McCartha, C. M. *Coord. Chem. Rev.* **1995**, *143*, 407–455. (b) Okuhara, T.; Mizuno, N.; Misono, M. *Adv. Catal.* **1996**, *41*, 113–252. (c) Kozhevnikov, I. V. *Chem. Rev.* **1998**, *98*, 171–198. (d) Katsoulis, D. E. *Chem. Rev.* **1998**, *98*, 359–388. (e) Neumann, R. *Prog. Inorg. Chem.* **1998**, *47*, 317–370. (f) Day, V. W.; Klemperer, W. G. *Science* **1985**, *228*, 533–541. (g) Coronado, E.; Gómez-García, C. J. *Chem. Rev.* **1998**, *98*, 273–296. (h) Müller, A.; Koegerler, P.; Kuhlmann, C. *Chem. Commun.* **1999**, 1347–1358.
(10) Mbomekalle, I. M.; Mialane, P.; Dolbecq, A.; Marrot, J.; Sécheresse, F.; Berthet, P.; Keita, B.; Nadjo, L. *Eur. J. Inorg. Chem.* **2009**, *34*, 5194–5204.
(11) (a) Tourney, C. M.; Tourné, G. F.; Zonnevijlle, F. *J. Chem. Soc., Dalton Trans.* **1991**, 143–155. (b) Ben-Daniel, R.; Weiner, L.; Neumann, R. *J. Am. Chem. Soc.* **2002**, *124*, 8788–8789. (c) Mialane, P.; Duboc, C.; Marrot, J.; Riviere, E.; Dolbecq, A.; Secheresse, F. *Chem.—Eur. J.* **2006**, *12*, 1950–1959. (d) Drewes, D.; Piepenbrink, M.; Krebs, B. *J. Cluster Sci.* **2006**, *2*, 361–374. (e) Keita, B.; Mialane, P.; Secheresse, F.; de Oliveira, P.; Nadjo, L. *Electrochem. Commun.* **2007**, *9*, 164–172. (f) Chen, W. L.; Chen, B. W.; Tan, H. Q.; Li, Y. G.; Wang, Y. H.; Wang, E. B. *J. Solid State Chem.* **2010**, *183*, 310–321.
(12) (a) Contant, R.; Thouvenot, R. *Can. J. Chem.* **1991**, *69*, 1498. (b) Keita, B.; Mbomekallé, I. M.; Nadjo, L.; Contant, R. *Electrochem. Commun.* **2001**, *3*, 267–273.
(13) Sheldrick, G. M. *SADABS; program for scaling and correction of area detector data*;University of Göttingen: Germany, 1997.
(14) Blessing, R. *Acta Crystallogr.* **1995**, *A51*, 33.
(15) Sheldrick, G. M. *SHELX-TL version 5.03, Software Package for the Crystal Structure Determination*; Siemens Analytical X-ray Instrument Division: Madison, WI, 1994.
(16) (a) Loose, I.; Droste, E.; Bösing, M.; Pohlmann, H.; Dickman, M. H.; Rosu, C.; Pope, M. T.; Krebs, B. *Inorg. Chem.* **1999**, *38*, 2688–2694. (b) Reinoso, S.; Vitoria, P.; Gutiérrez-Zorrilla, J. M.; Lezama, L.; Felices, L. S.; Beitia, J. I. *Inorg. Chem.* **2005**, *44*, 9731–9742. (c) Zhang, Z.; Qi, Y.; Qin, C.; Li, Y.; Wang, E.; Wang, X.; Su, Z.; Xu, L. *Inorg. Chem.* **2007**, *46*, 8162–8169.
(17) Keita, B.; Nadjo, L. *J. Electroannal. Chem.* **1988**, *243*, 87–103.
(18) Mbomekalle, I. M. Ph.D. dissertation, Université Paris-Sud XI, 2003.
(19) (a) Mbomekallé, I. M.; Keita, B.; Nadjo, L.; Contant, R.; Belai, N.; Pope, M. T. *Inorg. Chim. Acta* **2003**, *342*, 219–228. (b) Mbomekallé,

I. M.; Lu, Y. W.; Keita, B.; Nadjo, L. *Inorg. Chem. Commun.* **2004**, *7*, 86–90. (c) This last reference was cited by FinkeGraham, C. R.; Finke, R. G. *Inorg. Chem.* **2008**, *47*, 3679–3686. (d) Like the best of all the known procedures since the first one described by Wu in 1920: Wu, H. *J. Biol. Chem.* **1920**, *43*, 189–220.

(20) (a) Anderson, T. M.; Zhang, X.; Hardcastle, K. I.; Hill, C. L. *Inorg. Chem.* **2002**, *41*, 2477–2488. (b) Mbomekalle, I. M.; Keita, B.; Nadjo, L.; Neiwert, W. A.; Zhang, L.; Hardcastle, K. I.; Hill, C. L.; Anderson, T. M. *Eur. J. Inorg. Chem.* **2003**, 3924–3928.

(21) $\alpha\beta\beta\alpha$ is used in the sandwich-type structures to indicate the connectivity for the first cap−belt junction, the first and second belt−central M_4 junctions, and the second belt−cap junction, see ref 8i.

(22) Brese, N. E.; O'Keeffe, M. *Acta Crystallogr., Sect. B* **1991**, *47*, 192.

(23) Keita, B.; Mbomekalle, I. M.; Lu, Y. W.; Nadjo, L.; Berthet, P.; Anderson, T. M.; Hill, C. L. *Eur. J. Inorg. Chem.* **2004**, 3462–3475.

(24) Kambe, K *J. Phys. Soc. Jpn.* **1950**, *5*, 48.